DOI: 10.1002/fuce.201600034

Advanced Selectively Gas Permeable Anode Flow Field Design for Removal of Carbon Dioxide in a Direct Formic Acid Fuel Cell

S. Saeed[1], A. Pistono[2], J. Cisco[2], C. S. Burke[2], J. T. Clement[3], M. Mench[3], C. Rice[2,4]*

[1] Department of Mechanical Engineering, Tennessee Technological University, Cookeville, Tennessee 38505, USA
[2] Department of Chemical Engineering, Tennessee Technological University, Cookeville, Tennessee 38505, USA
[3] Department of Mechanical, Aerospace and Biomedical Engineering, University of Tennessee, Knoxville, 37996, USA
[4] Center for Manufacturing Research, Tennessee Technological University, Cookeville, Tennessee 38505, USA

Received February 26, 2016; accepted November 18, 2016; published online ■■■

Abstract

Direct formic acid fuel cells (DFAFCs) are electrochemical energy conversion devices well suited to power portable electronics, if researchers can harness their high theoretical efficiencies and address durability issues. To improve DFAFC efficiency, the mass transport of formic acid to the anode catalyst layer must be improved. Conventional serpentine anode flow field designs limit CO_2 product removal through a single flow field channel hindered by two-phase flow. Presented herein is an advanced electrically conductive, selectively gas permeable anode flow field (SGPFF) design that allows for efficient removal of CO_2 perpendicular to the active area near the location where it is formed in the catalyst layer. The anode plate design consists of two mating flow fields separated by semi-permeable separator to allow diffusive transport of CO_2. Herein, performance differences between a conventional liquid-fed flow field and an advanced SGPFF design are examined. Polarization curves revealed a 10% increase in performance of the SGPFF with confirmation of CO_2 removal within the gaseous side. A potential hold test at 0.3 V showed that the SGPFF sustained power generation for 9.5 times longer than that of the conventional anode flow field design in a dead-ended configuration, demonstrating the fixture's potential for sustained power generation.

Keywords: CO_2 Removal, Direct Formic Acid Fuel Cell (DFAFC), Flow Field, Fuel Cell Fixture, Portable Power

1 Introduction

Interest in proton exchange membrane fuel cells is growing to meet the increasing energy demands of portable electronic devices as the current power supply capabilities of today's state-of-the-art battery technologies are inadequate [1–4]. Currently, batteries with their finite storage capacity serve as the main power source for portable electronic devices. As researchers strive to meet the market's three dominant criteria of (i) reduced size, (ii) decreased weight, and (iii) increased power capacity, alternative energy conversion devices are being explored. Direct liquid fuel cells are electrochemical energy conversion devices that offer a viable approach to supplying today's energy demands by overcoming many of the challenges that batteries face, while maintaining a small footprint due to the high energy density of liquid fuels. For personal portable electronic devices, the ideal fuel cell types are based on proton exchange membranes due to the low temperature operation (<60 °C) restriction in order to meet criteria 1 and 2, above [1–4].

Fuel and catalyst selection is pivotal in controlling the overall kinetics and efficiency of the fuel cell. For portable electronics, methanol is the most investigated liquid fuel because of its relatively high power density and ease in handling. There are several drawbacks to direct methanol fuel cells (DMFCs): poor conversion efficiency, fuel crossover through the membrane,

[*] *Corresponding author, crice@tntech.edu*

moderate fuel toxicity, and lack of odor for leak detection [5]. Direct Formic Acid Fuel Cells (DFAFCs) offer an alternative to DMFCs by overcoming several limitations: higher conversion efficiency, lower fuel crossover, minimal toxicity and an identifiable odor for fast leak detection [6]. The anode reaction in a DFAFC requires three steps: (i) diffusion of formic acid (HCOOH) from the flow channels through the diffusion media and the three-dimensional porous anode catalyst layer to the electrochemically active catalyst sites, (ii) electro-oxidation at the catalyst surface site to produce carbon dioxide (CO_2), protons (H^+) and electrons, and (iii) diffusion of gaseous CO_2 back to the flow channels for subsequent removal via the flow field. There are two dominant electro-oxidation reaction pathways: (i) the direct reaction pathways with a reactive intermediate (Eq. (1)) and (ii) the indirect reaction pathway where surface poison adsorbed carbon monoxide (CO_{ads}) intermediate is formed (Eq. (2)) [7]

$$HCOOH \rightarrow \text{intermediates} \rightarrow CO_2 + 2H^+ + 2e^- \quad (1)$$

$$HCOOH \rightarrow CO_{ads} + H_2O \rightarrow CO_2 + 2H^+ + 2e^- \quad (2)$$

In the literature, recent advances in catalysis for DFAFCs have been demonstrated by several research groups [1–4, 8].

In DMFCs, a limited number of research activities have probed the adverse effect of carbon dioxide (CO_2) accumulation in the anode flow fields [9–13]. The accumulation of CO_2 in the anode flow field can degrade the performance of the fuel cell by disrupting the continuous stream of formic acid liquid fuel in the channels and thereby reducing the transport of fuel to catalyst reaction sites, due to two phases flow pressure drops [13, 14]. In the literature a few alternative DMFC flow field designs have been reported for efficient anode CO_2 product removal by either altering the number of serpentine flow field channels [12], selective removal within the flow profile through a non-conductive selectively permeable Teflon membrane [13, 15, 16], tapered geometry of the flow field [14, 17], and hydrophobic coatings of the channels [18–20]. The hydrophobic coatings were shown to attract the insoluble CO_2 bubbles to facilitate removal through the channels. The issue not addressed with the non-conducting membrane separator is lack of axial electron transfer across a two dimensional geometric area of the fuel cell. To circumvent CO_2 accumulation in the liquid feed of our DFAFC and to minimize the issues associated electron conduction through a non-conductive Teflon membrane the work presented herein is for a conductive selectively gas permeable flow field (SGPFF) design that was developed in-house. This SGPFF design could also be applied to DMFCs.

In this work, we report on an advanced SGPFF design allows for near site CO_2 bubble removal from the two-phase CO_2/formic acid flow present within the anode flow channel via a hydrophobic electrically conductive semi-permeable diffusion layer. Herein, DFAFC performance is compared to a standard solid plate anode flow field for the advanced SGPFF design with alternative semi-permeable materials. Specifically, power generation during a potentiostatic hold at 0.3 V is evaluated for sustained power generation capabilities. The CO_2 removal rate through the gaseous-side of the advanced SGPFF was also evaluated.

2 Experimental

2.1 Fuel Cell

The membrane electrode assembly was prepared by spraying the anode catalyst layer from an ink suspension containing carbon supported Pt(50 wt.%)/Ru(25 wt.%) alloy catalyst (Alfa Aesar HiSpec, 12100) with 30wt.% Nafion® onto a Nafion® HP proton exchange membrane (Ion Power, Inc.) to a final catalyst loading of 0.16 mg_{PtRu} cm^{-2}, measured gravimetrically. The ink was comprised of 150 mg Pt/Ru/C catalyst, 0.9 mL 18MΩ-cm Millipore water, 1.8 mL methanol, 0.87 mL of 5 wt.% 1100EW Nafion® suspension (Ion-Power, Inc., D521). A Pt containing gas diffusion electrode (Alfa Aesar, 045374) was used as the cathode and a thin layer of 5 wt.% Nafion® suspension was used as adhesive between the cathode gas diffusion electrode and the membrane interface to ensure good proton conductivity.

2.2 Fuel Cell Fixture

During the course of the experiments, three different anode separator configurations with 5 cm^{-2} active area were used with the same cathode flow field and endplate design from Fuel Cell Technologies. All flow patterns are single path serpentine with a geometrical cross-sectional area of 1 mm^2. A standard solid plate single fuel cell hardware (Fuel Cell Technologies) was used for conditioning with humidified gaseous reactants. To run formic acid on the anode and eliminate contamination of the fuel due to corrosion of the aluminum endplate, Fuel Cell Technologies designed the anode feed to directly enter the back of the flow field via rigid Teflon® tubes sealed with compression fittings. Herein, DFAFC tests are performed on two different types of anode flow fields within Fuel Cell Technologies DFAFC endplate: (i) the standard solid plate flow field (Figure 1A) and (ii) the advanced SGPFF design (Figure 1C). The semi-permeable flow field separates liquid formic acid and gaseous CO_2. This custom design consists of 3-components: (a) carbon composite liquid-side flow field, (b) hydrophobic semi-permeable separator, and (c) carbon composite gaseous-side flow field. The carbon composite was machined from BMC 940 (Bulk Molding Compounds, Inc.). The border separator is used to ensure uniform compression under applied axial load. Three hydrophobic semi-permeable separators are presented as part of this study. Each separator had two layers consisting of a hydrophobic macroporous carbon fiber substrate (treated with polytetrafluoroethylene (PTFE)) coated with a microporous carbon layer (MPL) (SGL Group, Inc., 10BC, 25BC, and 25CC). The MPL was positioned facing the liquid interface. Characteristics of the separators are listed in Table 1.

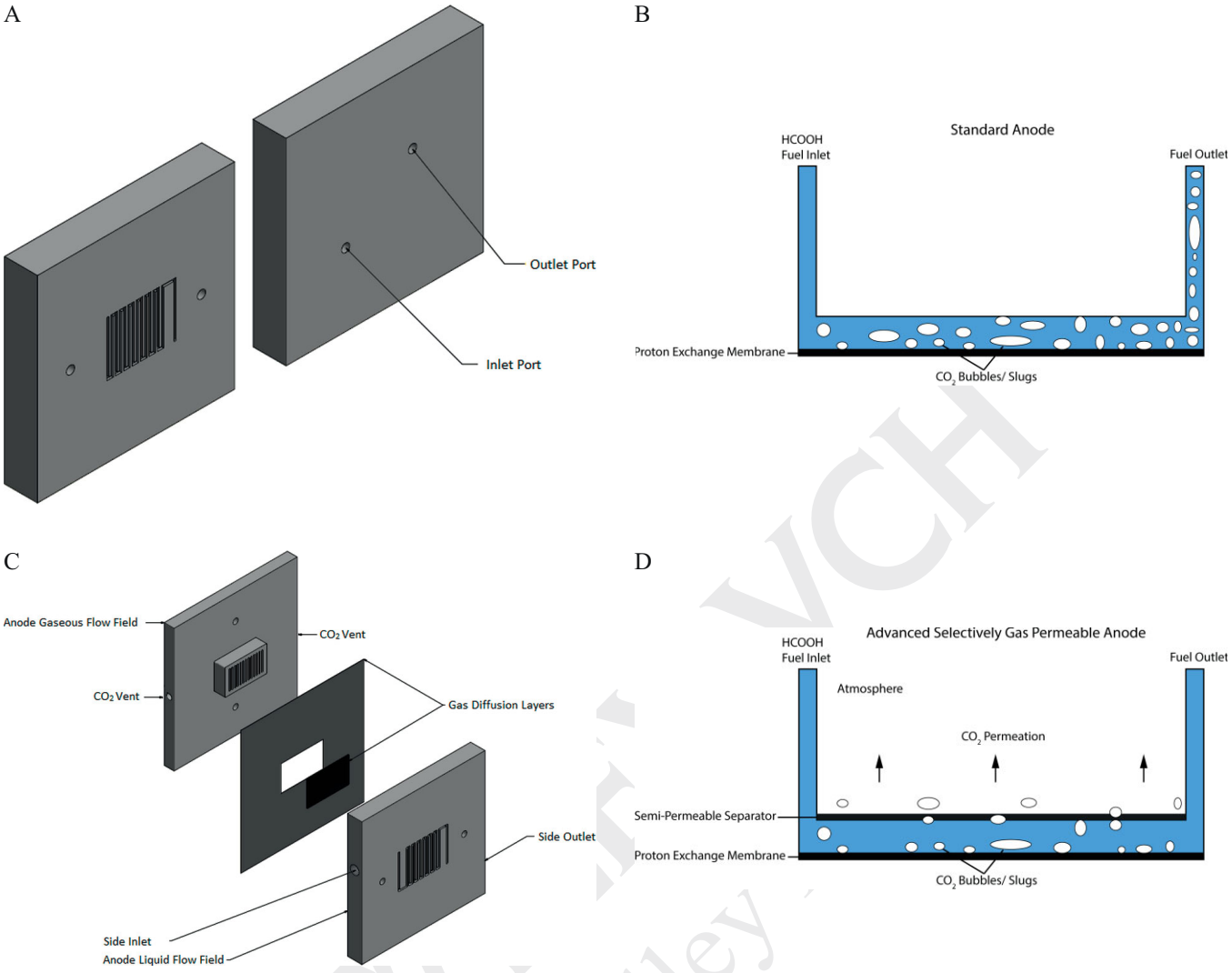

Fig. 1 Fuel Cell Technologies Inc. conventional flow field design (A–B) versus an advanced selectively gas permeable anode flow field design (C–D) consisting of the liquid flow field and the gaseous flow field separated by a semi-permeable separator for selective CO_2 transport. Channel cross-sectional view shows (B) the limitation of CO_2 removal for the conventional flow design vs. (D) the advanced selectively gas permeable design.

Table 1 Gas Diffusion Layers (GDL) tested for the varying substrate and microporous layer (MPL) hydrophobicity, as supplied by the manufacturer.

SGL Carbon Paper GDL	MPL	PTFE / wt.%	Uncompressed Porosity / %	Air Permeability / $cm^3\ cm^{-2}\ s^{-1}$	Uncompressed Thickness / µm
10BC	Yes	5	82	1.45	420
25BC	Yes	5	80	1.0	235
25CC	Yes	10	N/A	N/A	235

2.3 Instrumentation

A Scribner 850e test station was used to control gas flow, temperatures and load during polarization curve and constant voltage tests. A Solartron 1287 potentiostat was used to perform linear sweep voltammetry to remove adsorbed CO to regenerate the anode surface (data not shown). A Hiden HPR 20 residual gas analyzer was used to examine the gas effluent from the semi-permeable anode flow field fuel cell fixture.

2.4 Conditioning

To condition the catalyst layer, the dual-gas feed fuel cell fixture was operated at a temperature of 70 °C with 0.2 L min^{-1} hydrogen flowing through the anode and 0.5 L min^{-1} of either nitrogen or air (21% O_2 in N_2 balance) flowing through the cathode at 64% relative humidity. All gasses used within this study are ultra-high purity supplied by Airgas. The cell was conditioned by cycling the cathode between nitrogen and air at open circuit voltage, and subsequently performing polarization curves until performance stabilized.

2.5 Formic Acid Performance Testing

Identical tests were performed in both the standard DFAFC and semi-permeable fixtures. The cell was maintained at 40 °C. Liquid was delivered through the anode flow field at 2.5 mL min^{-1} with a Masterflex C/L peristaltic pump: flowing either 18MΩ-cm Millipore water or 5M formic acid (Sigma Aldrich, 09676). The cathode feed was humidified to 55% relative humidity and the air flow rate was 0.5 L min^{-1}. The voltage hold at 0.3 V was performed while the anode was dead-ended with gravity-fed formic acid. To recover performance loss due to intermediate accumulation from the indirect reaction pathway, CO-stripping linear sweep voltammograms were run between experiments. These were performed with water verses a dynamic hydrogen electrode (DHE) on the cathode, established by flowing 4% H_2 in a N_2 balance at 0.1 L min^{-1}, from 0.02 V to 0.8 V at 100 mV s^{-1}, results not shown. On Pt electrocatalyst the adsorbed CO intermediate is converted to gaseous CO_2 in the presence of adsorbed hydroxyl (OH_{ads}) species. Potentials greater than 0.4 V are required to convert H_2O into OH_{ads} [21].

3 Results and Discussion

3.1 Anode Flow Field Design

The anode flow field design constraints required maintaining key characteristics to ensure comparability to the Fuel Cell Technologies fixtures standard flow field dimensions: high electrical conductivity, minimal (ideally zero) formic acid permeation through or around the semi-permeable separator and optimal channel geometry. To structurally constrain the semi-permeable separator and maintain high electrical conductivity, a three layer anode flow field was designed with two graphite mating plates sandwiching the separator material.

The anode flow field designs evaluated within this study are presented in Figure 1A–D. Figure 1A shows the conventional serpentine channel anode flow field. Figure 1B is a schematic representation of a single channel cross-section of the conventional solid plate flow field design during high load operation of the direct formic acid fuel cell (DFAFC). It illustrates that CO_2 removal only occurs through the fuel outlet port as a void volume in the liquid fuel. Since gas-phase density is several hundreds of times lower than liquid phase density, the volumetric ratio of gas increases greatly toward the cell exit, which can block the fuel transport to the active catalyst sites over time. The advanced SGPFF anode design minimizes void volumes by selective transport of gas-phase out of the fuel flow field. The advanced SGPFF in Figure 1C consists of two mating graphite plates: 1) a liquid flow field that transports the fuel in and out and 2) a gaseous flow field that allows for the transportation of gaseous CO_2 to the atmosphere. These plates are separated by a hydrophobic, semi-permeable diffusion media which acts as a barrier to formic acid in the liquid flow field, yet allows for CO_2 permeation between the plates. Figure 1D depicts the near site of formation egress of CO_2 through the semi-permeable separator and the reduction of void volume in the liquid feed.Initial prototypes showed that inlet/outlet tubes passing through the endplate, as in the standard flow field, incurs leakage of fuel due to the additional sealing required for the two mating flow field plates and for the tubes passing through the gaseous flow field plate. To minimize leakage, the inlet/outlet ports were integrated into the sides of the liquid flow field, thereby bypassing the gaseous flow field, as shown in Figure 1C. In addition to minimizing fuel leakage, it decreased flow field resistance due to reduced use of non-conductive sealing materials and allowed for a wider range of semi-permeable separator thickness between the mating plates. The land and channel geometry of the serpentine liquid-side of the flow field was constrained to the equivalent dimensions of the standard solid plate flow field geometry to minimize any variables that could lead to performance differences not associated with CO_2 removal. Electrical conductivity between the plates through multiple point contact was crucial to maintaining a lower flow field ohmic resistance. Comparable resistance values were achieved with the advanced SGPFF being slightly higher (102 mOhm-cm^2) compared to the baseline flow field (92 mOhm cm^2), as measured via current interrupt during the polarization curves.

3.2 Semi-Permeable Separator

The selection criteria of the semi-permeable separator included: high electrical conductivity, impermeability of liquids, and permeability of gases (CO_2). In a typical H_2/O_2 fuel cell configuration, multilayer hydrophobic GDLs provide a porous structure for gas and vapor water transport [22]. They deliver reactants to, and products away from, the electrodes, as well as provide high electrical conductivity with low contact resistance and appropriate heat transfer [23]. There are multiple crucial parameters that effect the performance of a GDL such as: thickness, hydrophobicity, pore size distribution and gas permeability [24]. Previous studies of GDLs have shown that increasing the hydrophobic PTFE content on the carbon fiber substrate resulted in an increase in the water transport resistance through the GDL [25,26]. The effect of Teflon® content in a gas diffusion media reveals that with increasing hydrophobicity, a decrease in permeability and pore diameter is observed due to Teflon® coating on the walls of the pores of the diffusion media [27]. Additionally, studies have shown the effects of MPL carbon loading on fuel cell performance that allow for effective liquid management [28]. It was reported that GDLs coated with a MPL also decreases the average pore diameter of the porous substrate and that low levels of carbon loading results in water flooding in the carbon fiber substrate which impeded oxygen diffusion [29]. Since the semi-permeable separator needs to be impermeable to liquids, but permeable to gases, it is then significantly affected by the MPL and hydrophobicity. Therefore, it was hypothesized that integration of hydrophobic GDLs with a MPL as semi-permeable separators between the two mating flow fields would selectively retain the aqueous formic acid solution by acting as

a barrier, while permitting diffusion of CO_2 adjacent to the flow channel, thereby removing it from the two-phase flow of the formic acid stream. Table 1 lists the carbon paper GDL supplier provided material characteristics that were tested in the advanced SGPFF as part of this study [30, 31]. The first letter designates the degree of hydrophobic treatment (PTFE content) for the substrate and the second letter indicates whether or not the GDL contains a micro-porous layer (MPL). GDLs 25BC and 25CC were used to evaluate the effect of hydrophobicity levels of the substrate on performance, while GDL 10BC was used to evaluate the effect of thickness along with its higher air permeability and porosity. The change in porosity and permeability due to compression under the applied axial load was identical for all GDLs tested and is assumed to have a lower than 20% change in tortuosity [32].

3.3 DFAFC Performance

DFAFC ohmic resistance compensated (iR corrected) polarization curves (PCs) with CO_2 partial pressures are shown in Figure 2 for the standard anode flow field and three variations of the advanced SGPFF with different separator materials. Characteristics of the three types of separator materials studied, such as porosity, permeability, Teflon® (PTFE) content in macroporous layer and overall thickness are summarized in Table 1. The PCs of the advanced SGPFF with the separators shows a ca. 10% increase in performance in voltage response compared to the standard fixture at a load of 480 mA cm^{-2}. A significant reduction in the abundance of CO_2 bubbles was observed in the outlet stream of the fixture as a result of the effective two phase flow separation and egress of CO_2. The polarization performance of the standard fixture can be seen to initially decline in the ohmic region with a continuous drop leading into the mass transport region, Figure 2A. The advanced SGPFF shows better performance in the mass transport region with minor differences between the various semi-permeable barriers. The maximum power density increased by over 6%. While obtaining polarization curve results, a residual gas analyzer was used to indicate CO_2 levels inside the gaseous flow field chamber to verify the effectiveness of CO_2 removal. The partial pressure of CO_2 vs. applied current density in Figure 2B shows a gradual rise of CO_2 at the start of the polarization sweep, reaching a plateau at the highest current densities. This maximum CO_2 removal plateau appears to be material dependent, as the GDL with the thicker hydrophobic substrate has 4% less measured CO_2 at identical production rates, attributed slower removal rate due to the extended torturous path length.

In the mass transport region of the polarization curve in Figure 2A for the SGL 25BC, a minor upward shift is noted compared to the SGL 25CC and 10BC. The difference in performance compared to the SGL 25CC could possibly be attributed to the lower hydrophobicity of the SGL 25BC associated with having a lower wt.% of PTFE. However, at the end of the polarization curve test, the SGL 25BC was inspected and it was observed that minor droplets were beginning to form on the gaseous flow field side, suggesting that liquid permeation through the pores was occurring. Meanwhile, SGL 25CC, with

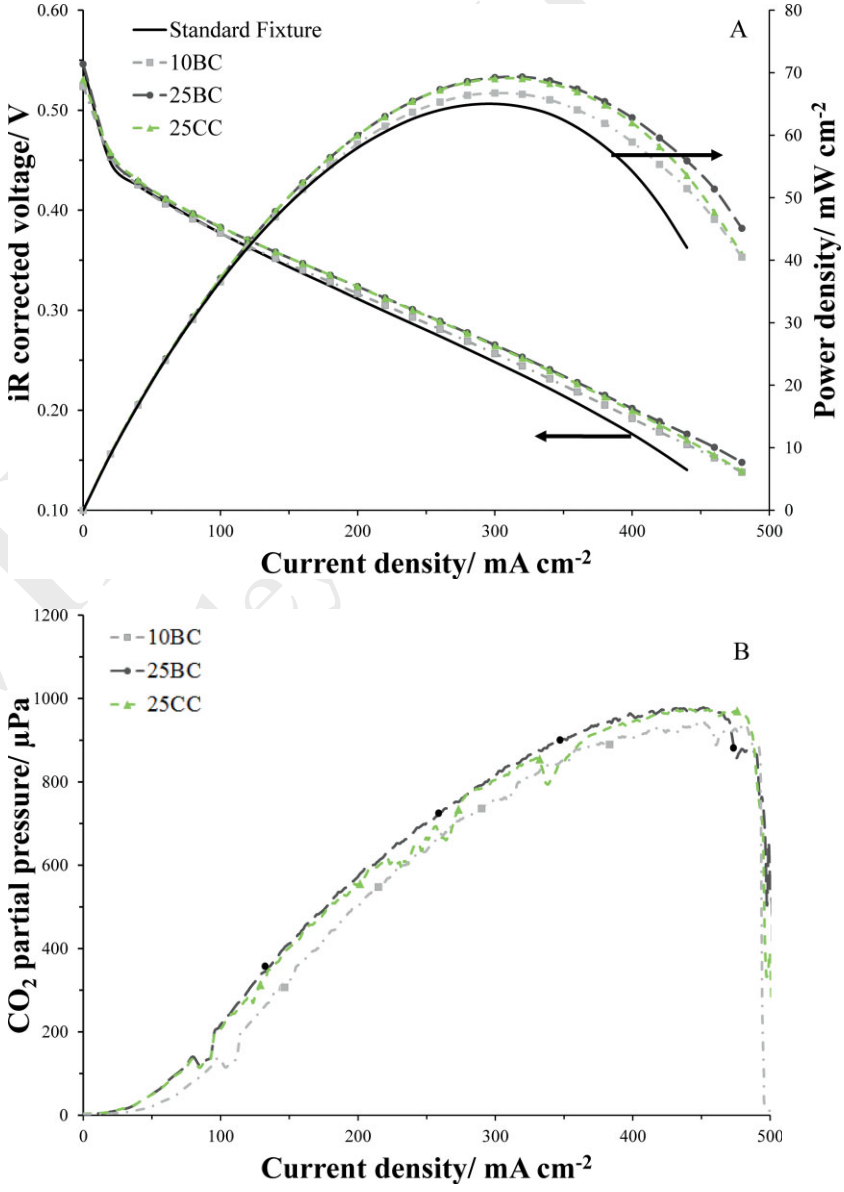

Fig. 2 DFAFC polarization curves comparing the standard solid plate flow field to the advanced anode selectively gas permeable flow field (SGPFF) at 40 °C with 5 M formic acid (2.5 mL min^{-1}) on the anode and air (21% O_2, 0.5 L min^{-1}) as the cathode feed. The separators in the anode SGPFF were SGL 10BC, 25BC, and 25CC. (A) Polarization and power density and (B) CO_2 partial pressure.

ORIGINAL RESEARCH PAPER

higher %wt PTFE, showed complete resistance to formic acid permeation during the tests. With liquid penetration that occurred in the SGL 25BC, one would have expected to see a noticeable decline in performance in the mass transport region and the egress of CO_2 as a result of the liquid hindering the transport of gaseous molecules through the separator. However, this was not the case found in either the CO_2 partial pressures or the polarization curves, which could suggest that the liquid transport was too minor to have any adverse effects on mass transport and that it occurred at a very late stage and at a high current density of the polarization curve test.

The performance of the SGL 10BC shows a drop in the activation region similar to the standard DFAFC fixture, but subsequently shows ohmic and mass transport performance similar to SGL 25BC despite the higher air permeability and porosities, suggesting lower concentrations of formic acid within the catalyst layers. The SGL 10BC was also susceptible to liquid permeation, similar to SGL 25BC, as droplets began to form on the surface of the GDL at the end of the polarization curve test. The minor change in the activation region and the liquid permeation could possibly be a result of the nearly doubled thickness of the SGL 10BC that resulted in a higher compression on fiber substrate of the GDL surface, thereby reducing porosity and permeability. The increased compression due to the greater thickness of SGL 10BC causes the SGPFF to act more like the conventional flow field due to CO_2 retention ~~in the~~ on the liquid side and hence reduces the formic acid concentration within the catalyst layer. Additionally, the higher thickness could have caused intrusion in the flow field channels due to deflection, thus reducing the cross-sectional area of the channel, which reduces mass transport and decreases the amount of formic acid within the cell for reaction.

Potentiostatic holds were performed at 0.3 V with formic acid and air for 15 minutes while the anode flow fields were in a dead-ended configuration. Figure 3A shows that the advanced SGPFF was able to sustain currents for roughly 9.5 times longer than the baseline flow field with no signs of liquid permeation to the gas-phase side. The performance decay is partially due to poisoning of the catalyst, as Pt/Ru alloy is known to significantly participate in the formic acid indirect reaction pathway accumulating CO_{ads}, thereby halting further reaction. However, the potentiostatic hold demonstrates the sustained power generation ability of the advanced SGPFF in a dead-end fed configuration. During the potential holds, within the first few minutes of testing with the standard flow field, backflow of the fuel due to production of CO_2 was observed concurrently with the sharp decrease in current density. This was not evident in the advanced SGPFF due to removal of CO_2 through the semi-permeable separator/gaseous flow field. In Figure 3B, the advanced SGPFF shows CO_2 removal rates trending with the current density generations profiles. The SGL 10BC and 25 CC have identical current density and CO_2 removal rates profiles. However, the SGL 25BC has a 15% lower maximum current density, but a 6% increase in the amount of CO_2 released through the SGPFF. Current density for SGL 25BC is sustained at a higher rate after 4 min of being on hold for an extended

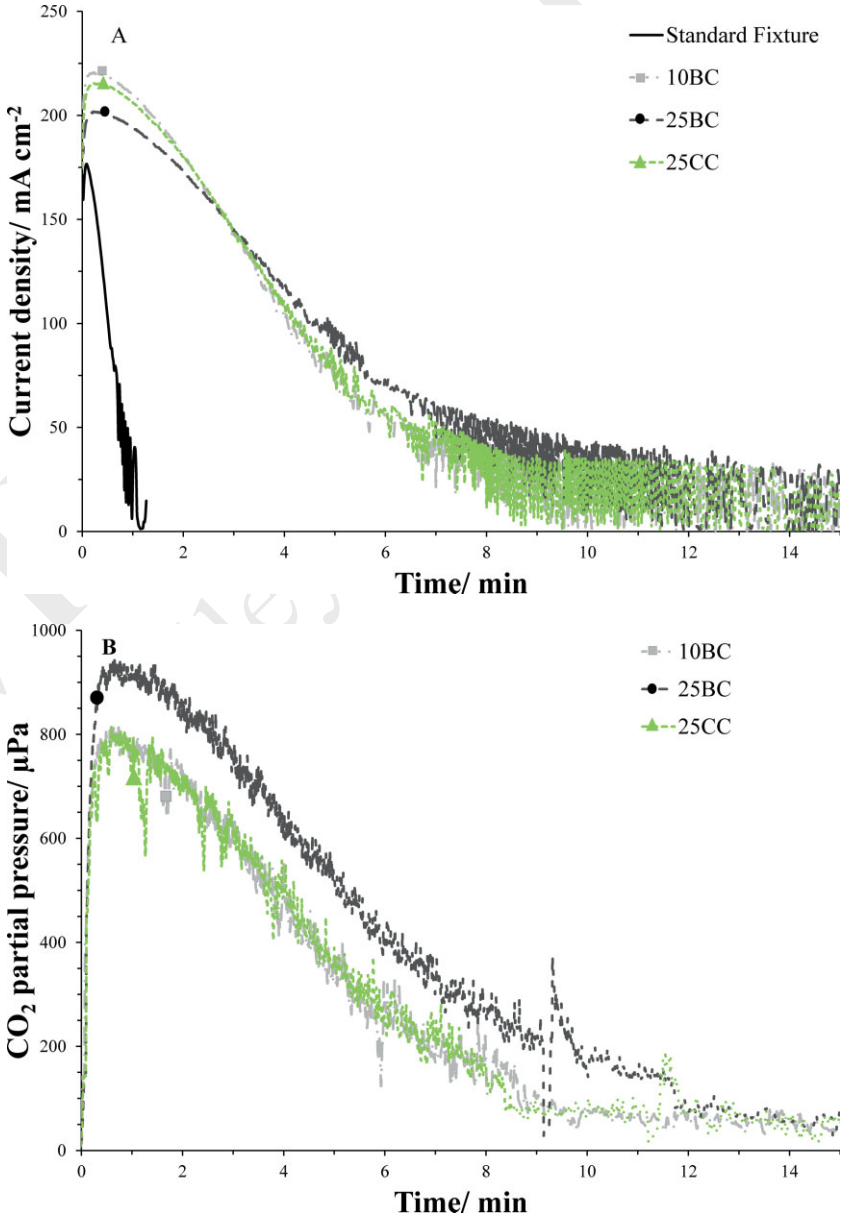

Fig. 3 Potentiostatic hold at 0.3 V comparing the standard solid plate flow field to the anode SGPFF at 40 °C with 5M formic acid (2.5 mL min^{-1}) on the anode and air (21% O_2, 0.5 L min^{-1}) as the cathode feed. The separators in the anode SGPFF were SGL 10BC, 25BC, and 25CC. (A) Current density and (B) CO_2 partial pressure.

time until around 12 min. This design is compatible with fuel cell stack architectures as a CO_2 manifold could be integrated in with the removal from the sides.

Future work is under way to explore alternative separator materials with super hydrophobicity (contact angle >150°) characteristics as the advanced SGPFF is limited by the performance of the semi-permeable barrier and is restricted to low power application. It was observed that at current densities beyond 480 mA cm^{-2} the semi-permeable barriers could not restrict liquid permeation due to electro-osmosis through the porous material, thus resulting in transport of the liquid alongside the bulk CO_2 flow through the separator layer. This allowed the two phase flow to pass into the gaseous flow field, which negatively impacted the performance. To extend the CO_2 removal capabilities of the separator materials, thinner substrates will be investigated and the impact of applied vacuum to the gas side will be explored.

4 Conclusions

This study investigates facilitated CO_2 removal from the anode channels of a DFAFC through an advanced selectively gas permeable flow field (SGPFF) design consisting of two mating plates separated by semi-permeable diffusion media. One plate acts as a liquid flow field that transports the fuel and the other acts as a gaseous flow field, allowing for direct CO_2 removal to the atmosphere near site of formation. The advanced SGPFF showed a ca. 10% increase in performance during polarizations tests across all semi-permeable barriers tested when compared to the conventional flow field design. In a dead-ended configuration during a 0.3 V potentiostatic hold, the advanced flow field design sustained a higher power for roughly 9.5 times longer than that of the conventional anode flow field. Residual gas analysis of the gas-phase side indicated load-dependent levels of CO_2 production, confirming the ability of the advanced fixture to selectively remove CO_2. The application of this advanced SGPFF is presently limited to low power applications due to the liquid retention limits presented by the semi-permeable barriers under high current densities.

Acknowledgements

We gratefully acknowledge the support of this work by the NSF-funded TN-SCORE program, NSF EPS-1004083, under Thrust 2. TN-SCORE's funding of 2013 summer REU for Mr. Saeed at the University of Tennessee at Knoxville with Dr. Mench. Dr. Rice would like to thank TN-SCORE for the residual gas analyzer equipment acquisition. Dr. Rice gratefully acknowledges TTU 2012 Faculty Research Grant for initial funding of this project.

References

[1] S. Z. Rejala, M. S. Masdarab, S. K. Kamarudina, *Energy and Environmental Engineering Journal* **2013**, *2*, 7.
[2] H. Jeon, B. Jeong, J. Joo, J. Lee, *Electrocatalysis* **2015**, *6*, 20.
[3] C. A. Rice, A. Bauskar, P. G. Pickup, Recent advances in electrocatalysis of formic acid oxidation, in *Electrocatalysis in Fuel Cells: A Non and Low Platinum Approach, Lecture Notes in Energy 9*, (Ed: M. Shao), ~~Publisher, Location??~~, **2013**, p. 69.
[4] X. Yu, P. G. Pickup, *J. of Power Sources* **2008**, *182*, 124.
[5] H. A. Gasteiger, J. Garche, in: *Handbook of Heterogeneous Catalysis*, (Ed: G. Ertl), ~~Publisher, Location??~~, **2008**, p. 3081.
[6] B. Beden, F. Hahn, S. Juanto, C. Lamy, J. M. Leger, *J. of Electroanalytical Chemistry and Interfacial Electrochemistry* **1987**, *225*, 215.
[7] A. Capon, R. Parsons, *J. of Electroanalytical Chemistry and Interfacial Electrochemistry* **1973**, *45*, 205.
[8] A. S. Bauskar, C. A. Rice, *Electrochimica Acta* **2012**, *62*, 36.
[9] P. Argyropoulos, K. Scott, W. M. Taama, *Electrochimica Acta* **1999**, *44*, 3575.
[10] G. Q. Lu, C. Y. Wang, *J. of Power Sources* **2004**, *134*, 33.
[11] H. Yang, T. S. Zhao, Q. Ye, *J. of Power Sources* **2005**, *139*, 79.
[12] V. B. Oliveira, C. M. Rangel, A. M. F. R. Pinto, *Chemical Engineering Journal* **2010**, *157*, 174.
[13] S. Jung, Y. Leng, C.-Y. Wang, *Electrochimica Acta* **2014**, *134*, 35.
[14] M. Li, J. Liang, C. Liu, G. Sun, G. Zhao, *Sensors* **2009**, *9*, 3314.
[15] G. Beckman, W. P. Acker, *WO2002045196A2*, **2002**.
[16] M. S. Defilippis, *WO2003077342A2*, **2003**.
[17] C. Litterst, S. Eccarius, C. Hebling, R. Zengerle, P. Koltay, *Journal of Micromechanics and Microengineering* **2006**, *16*, S248.
[18] T. Hutzenlaub, N. Paust, R. Zengerle, C. Ziegler, *Journal of Power Sources* **2011**, *196*, 8048.
[19] D. D. Meng, C.-J. Kim, *Lab Chip* **2008**, *8*, 958.
[20] D. D. Meng, C. J. Kim, *Journal of Power Sources* **2009**, *194*, 445.
[21] A. Hamnett, *Catalysis Today* **1997**, *38*, 445.
[22] A. Arvay, E. Yli-Rantala, C. H. Liu, X. H. Peng, P. Koski, L. Cindrella, P. Kauranen, P. M. Wilde, A. M. Kannan, *J. of Power Sources* **2012**, *213*, 317.
[23] E. C. Kumbur, K. V. Sharp, M. M. Mench, *J. of Power Sources* **2007**, *168*, 356.
[24] S. Park, J.-W. Lee, B. N. Popov, *International J. of Hydrogen Energy* **2012**, *37*, 5850.
[25] S. Park, J.-W. Lee, B. N. Popov, *J. of Power Sources* **2008**, *177*, 457.
[26] G. Lin, T. V. Nguyen, *J. of the Electrochemical Society* **2005**, *152*, A1942.
[27] G.-G. Park, Y.-J. Sohn, T.-H. Yang, Y.-G. Yoon, W.-Y. Lee, C.-S. Kim, *J. of Power Sources* **2004**, *131*, 182.

[28] K. T. Cho, M. M. Mench, *Physical Chemistry Chemical Physics* **2012**, *14*, 4296.

[29] S. Park, J.-W. Lee, B. N. Popov, *J. of Power Sources* **2006**, *163*, 357.

[30] Ion-Power, Sigracet, GDL 24 & 25 Series Gas Diffusion Layer, http://www.ion-power.com/res/Sigracet/GDL_24_25_Series_07.pdf

[31] Ion-Power, Sigracet, GDL 10 Series Gas Diffusion Layer, http://www.ion-power.com/res/Sigracet/GDL_10_Series_07.pdf

[32] J. Bear, *Dynamics of Fluids in Porous Media*, Ed. ~~Publisher, Location??~~, **1988**.